gain, the receiver sensitivity was improved by 7 dB, resulting in a sensitivity of –26.2 dBm. The 4 dB power penalty is caused by the optical noise added by the VCSOA. No error floor was observed. The eye pattern at a BER of 10^{-9} is also shown in Figure 3. Excess noise from the optical amplification is visible in the high level.

4. Conclusions

We have demonstrated optical preamplification at 10 Gb/s using a VCSOA. The VCSOA has a narrow bandwidth of 37 GHz and functions as an amplifying filter. Operating the VCSOA at 11 dB fiber-fiber gain resulted in a 7 dB improvement in receiver sensitivity. These results suggest that VCSOAs are potential low-cost alternatives to more expensive preamplifiers such as fiber amplifiers. The combined functionality preamplifier-filter is especially attractive for WDM applications where channel selection is needed. Our present device is optimized for reflection mode operation; better isolation of adjacent channels can be obtained using transmission mode operation. Interesting possibilities for future devices include integration of vertical-cavity amplifying filters with photodetectors, either as single devices or 2-dimensional arrays for parallel applications. Tunable receivers could be realized by employing micro electromechanical systems (MEMS), similar to what is being used for tunable VCSELs.[5]

References

1. R.I. Laming, A.H. Gnauck, C.R. Giles, M.N. Zervas, D.N. Payne, "High-Sensitivity Two-Stage Erbium-Doped Fiber Preamplifier at 10 Gb/s," IEEE Photonics Technol. Lett., **4,** 1348–1350 (1992).
2. T. Ducellier, R. Basset, J.Y. Emery, F. Pommereau, R. N'Go, J.L. Lafragette, P Aubert, P. Doussière, P. Laube, L. Goldstein, "Record low noise factor (5.2 dB) in 1,55 μm bulk SOA for high bit rate low-noise preamplification," in Tech. Dig. ECOC '96, **3,** 173–176 (1996).
3. F. Koyama, S. Kubota, K. Iga, "GaAlAs/GaAs active filter base on vertical cavity surface emitting laser", Electron, Lett., **27,** 1093–1095 (1991).
4. A. Black, A.R. Hawkins, N.M. Margalit, D.I. Babic, A.L. Jr. Holmes, Y.-L. Chang, P. Abraham, J.E. Bowers, E.L. Hu, "Wafer fusion: materials issues and device results", IEEE J. Select. Topics Quantum Electron., **3,** 943–951, (1997).
5. D. Vakshoori, J.H. Zhou, M. Jiang, M. Azimi, K. McCallion, C.C. Lu, K.J. Knopp, J. Cai, P.D. Wang, P. Tayebati, H. Zhu, P. Chen, "C-band tunable 6 mW vertical-cavity surface emitting lasers", in Technical Digest Optical Fiber Communication Conference (OFC 2000), post-deadline session, PD13 (2000).

TuW6 **5:45 pm**

High-performance 1.55 μm Resonant Cavity Enhanced Photodetector

Ibrahim Kimukin, Necmi Biyikli, Ekmel Ozbay, *Bilkent University, Department of Physics 06533 Ankara, Turkey, Email: kimukin@fen.bilkent.edu.tr*

High-performance photodetectors operating at 1.55 μm wavelength are required for ultrafast photodetection in optical communication, measurement, and sampling systems. The photodiode performance is measured by the bandwidth-efficiency product (BWE) and is limited for conventional vertically illuminated photodiodes (VPDs) due to the bandwidth-efficiency tradeoff.[1] This tradeoff arises from the fact that the quantum efficiency and bandwidth of a conventional VPD, have inverse dependencies on the photoabsorption layer thickness. To overcome the BWE limitation for such conventional VPDs, two alternative detection schemes were offered: edge-coupled photodiodes and resonant-cavity-enhanced photodiodes (RCE-PDs). Both PD structures have demonstrated excellent performances and are potential candidates as photodetectors for future high bitrate optical communication systems.[2–6] The ease of fabrication, integration, and optical coupling makes the RCE-PD more attractive for high-performance photodetection.

We used the transfer matrix method to design the epilayer structure and to simulate the optical properties of the photodiode. The bottom Bragg mirror is made of 25 pair quarter-wave stacks (InAlAs/$In_{0.53}Al_{0.13}Ga_{0.34}As$) centered at 1550 nm. The structure was grown by solid-source MBE on semi insulating InP substrate. The details of the epitaxial structure we have used is given in Table 1. The reflectivity measurements showed that the thickness of the epilayers were 3.7% thicker than our design. This shifted the high reflectivity center of the bottom mirror to 1610 nm.

The samples were fabricated by a microwave-compatible process. First ohmic contact to n+ layer was formed by recess etch with a phosphoric acid based etchant that was followed by a self-aligned Au-Ge-Ni liftoff. The p+ ohmic contact was achieved by Ti/Au liftoff. The samples were then rapid thermal annealed at 400°C. Using an isolation mask, we etched away all of the epilayers down to the undoped layer except the active areas. Then we evaporated Ti/Au interconnect metal which formed the coplanar waveguide (CPW) transmission lines on top of the semi-insulating substrate. Silicon nitride layer was deposited using PECVD which is used for both passivation and the insulater layer of metal-insulator-mater capacitors. Finally, a 0.7 mm Au layer was evaporated as an airbridge to connect the center of the CPW to the p+ ohmic metal.

Photoresponse measurements were carried out in the 1530–1630 nm range using a tunable laser source. The output of the laser was coupled to a single mode fiber. The light was delivered to the devices by a lightwave fiber probe, and the electrical characterization was carried out on a microwave probe station. The top p+ layers were

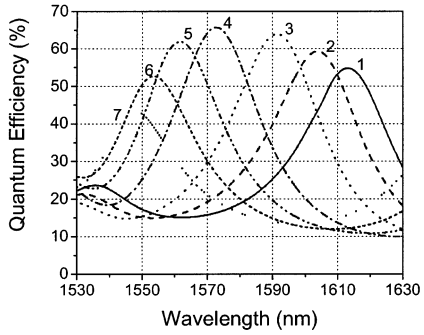

(a)

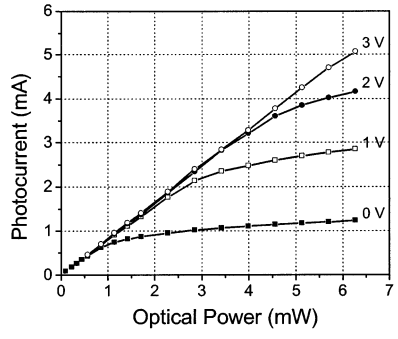

(b)

TuW6 Fig. 1. (a) Spectral quantum efficiency measurements of the fabricated detectors after consecutive recess etches. (b) Optical input power versus photocurrent of the photodetector under various reverse biases.

recess etched in small steps, and the tuning of the resonance wavelength within the high reflectivity spectral region of the DBR was observed.

Fig. 1(a) shows the spectral quantum efficiency measurements of a device under 5 V reverse bias obtained by consecutive ~35 nm recess etches. The peak quantum efficiency increased up to 66% with tuning until the resonance wavelength reached 1572 nm. This increase was due to the increase of the absorption coefficient of InGaAs at shorter wavelengths. As we continued the recess etch, the peak quantum efficiency decreased due to the decrease of the reflectivity of the Bragg mirror. The resonance wavelength was tuned for a total of 47 nm (1538–1605 nm) while keeping the peak efficiencies above 60%. The peak efficiency was above 50% for the resonant

TuW6 Table 1. Epitaxial structure of the wafer

Material	Thickness (nm)	Doping (cm–3)
InGaAs	30	p+ 10^{19}
Graded Layer	30	p+ 10^{19}
InAlAs	210	p+ 10^{19}
InAlAs	50	n– 10^{16}
Graded Layer	30	n– 10^{16}
InGaAs	300	n– 10^{16}
Graded Layer	30	n– 10^{16}
InAlAs	60	n– 10^{16}
InAlAs	300	n+ 3×10^{18}
InAlAs	240	None
25 Pair InAlAs/InAlGaAs DBR	25 × (121/112)	None
InP Substrate	600 μm	Semi-insulating

wavelengths between 1550 and 1620 nm, corresponding to a tuning range of 70 nm.

The full width at half maximum (FWHM) of the devices was around 35 nm. The quantum efficiency measurements were done at 5 V reverse bias under 0.5 mW optical input power. When we increased the reverse bias beyond 3 V the active layer was fully depleted, and the quantum efficiency increased 6% with respect to zero bias. The responsivity of the PDs were also measured under various reverse biases up to 6 mW optical power, which was the maximum power that could be obtained from the laser. Fig. 1(b) shows the photocurrent versus input optical power at the resonance wavelength of 1572 nm. Under 3 V and higher reverse biases, the PDs had a linear photoresponse up to 6 mW optical power. At 6 mW optical power, the device exhibited a 5 mA photocurrent. The saturation was mainly due to the electric field screening caused by photo-generated carriers.[7]

High-speed measurements were made with a picosecond fiber laser operating at 1550 nm. The 1 ps FWHM optical pulses from the laser were coupled to the active area of the p-i-n photodiodes by means of a fiber probe. At zero bias, the response of the photodetectors had a long tail due to the diffusion of the carriers in the active layers. Measurements were done under bias to deplete the active layer completely and to get rid of the diffusion tail. Above 3 V reverse bias, we got a Gaussian response with a short tail. Fig. 2 shows the temporal response of a small area ($5 \times 5\ \mu m^2$) photodetector measured at 7 V bias by a 50 GHz sampling scope. The photodiode output had a 16 ps FWHM. The measured data was corrected by deconvolving the effect of the 40 GHz bias-tee. After the deconvolution, the device had a 3-dB bandwidth of 31 GHz. Larger area devices (80 μm^2) also showed similar responses, which showed that the temporal response was limited by the transport of the photogenerated carriers.

In conclusion, we have demonstrated high-speed, and high-efficiency resonant cavity enhanced (RCE) InGaAs based p-i-n photodetectors. A peak quantum efficiency of 66% was measured along with 31 GHz bandwidth, which corresponds to 20 GHz bandwidth-efficiency product. The photoresponse was linear up to 6 mW optical power, where the devices exhibited 5 mA photocurrent.

This work was supported by NATO Grant No. SfP971970, National Science Foundation Grant No. INT-9906220, Turkish Department of Defense Grant No. KOBRA-001 and Thales JP8.04

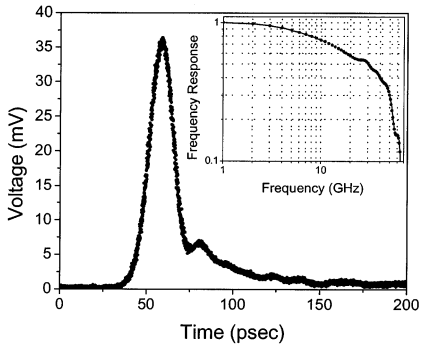

TuW6 Fig. 2. Temporal response of the photodetector with a 16 psec full width at half maximum. The inset shows the deconvolved frequency response obtained from the fast Fourier transform of the temporal dedetector response.

1. M.S. Unlu and S. Strite, "Resonant cavity enhanced (RCE) photonic devices," J. Appl. Phys. Rev., vol. **78,** no. 2, 607–639, (1995).
2. S.M. Spaziani, K. Vaccaro, and J.P. Lorenzo, "High-performance substrate-removal InGaAs Schottky photodetectors", *IEEE Photon. Technol. Lett.,* vol. **10,** no. 8, 1144–1146, (1998).
3. S.Y. Hu, j. Ko, and L.A. Coldren, "Resonant-cavity InGaAs/InAlGaAs/InP photodetector arrays for wavelength demultiplexing applications", *Appl. Phys. Lett.,* vol. **70,** no. 18, 2347–2349, (1997).
4. C. Lennox, H. Nie, P. Yuan, G. Kinsey, A.L. Holmes, B.G. Streetman, and J.C. Campbell, "Resonant-cavity InGaAs-InAlAs avalanche photodiodes with gain-bandwidth product of 290 GHz," *IEEE Photon. Technol. Lett.,* vol. **11,** 1162–1164, (1999).
5. E. Ozbay, I. Kimukin, N. Biyikli, O. Aytur, M. Gokkavas, G. Ulu, M.S. Unlu, R.P. Mirin, K.A. Bertness, and D.H. Christensen, "High-speed >90% quantum efficiency p-i-n photodiodes with a resonance wavelength adjustable in the 795–835 nm range," *Appl. Phys. Lett.,* vol. **74,** no. 8, 1072–1074, (1999).
6. Necmi Biyikli, Ibrahim Kimukin, Orhan Aytur, Mutlu Gokkavas, M. Selim Unlu, Ekmel Ozbay, "45-GHz bandwidth-efficiency resonant-efficiency-enhanced ITO-schottky photodiodes", *IEEE Photon. Technol. Lett.,* vol. **13,** no. 7, 705–707, (2001).
7. L.Y. Lin, M.C. Wu, T. Itoh, T.A. Vang, R.E. Muller, D.L. Sivco, and A.Y. Cho, "High-power high-speed photodetectors—Design, analysis, and experimental demonstration", *IEEE Trans. Microwave Theory. Tech.,* vol. **45,** no. 8, 1320–1331, (1997).

TuX

4:30 pm–6:00 pm
304 A–D

Network Design 2

Jane M. Simmons, *Corvis Corp., USA, Presider*

TuX1 **4:30 pm**

Routing power: a metric for reconfigurable wavelength add/drops

Mark D. Feuer and Daniel Al-Salameh, *JDS Uniphase Corp., 625 Industrial Way, Eatontown, NJ 07724, Email: mark.feuer@us.jdsuniphase.com*

Reconfigurable Wavelength Add/Drop Modules

Reconfigurable Wavelength Add/Drop Modules (RWADMs) make up the cores of Optical Add/Drop Multiplexers (OADMs), the network elements which will enable next-generation optical networking.[1–5] For the present work, we define the RWADM as a device comprising two logical input ports (IN and ADD) and two logical output ports (OUT and DROP), which has the ability to route selected wavelengths from either input port to either output port. The four logical ports of an WADM may be made up of more than one fiber each. For example, the DROP port may provide one fiber per wavelength or may use WDM to combine all dropped signals in a single fiber. Of course, a device with one multi-wavelength drop fiber can be converted into a device with many single-wavelength drop fibers (or vice versa) by appending a wavelength DMUX (MUX) to the drop fiber(s). For simplicity, this paper will concentrate on unidirectional WADMs which provide no wavelength conversion function.

First-generation optical networks have been based on fixed WADMs which add/drop one wavelength or a band of a few contiguous wavelengths at a given location. In contrast, the new generation of dynamic optical networks will require WADMs which are reconfigurable, operating under the control of network or element manager software. Using RWADMs, networks can provide flexible, efficient assignment of connection resources without terminating all channels at every node. In the following sections, we discuss some options for RWADMs, and present a figure of merit, the routing power, for quantifying the effectiveness of such RWADMs in network applications.

Global Routing Power

To first order, capacity of RWADMs is specified by the number N of wavelengths in the WDM spectrum at the IN and OUT ports and the maximum number K of wavelengths allowed for simultaneous add/drop. (We assume $K_{add} = K_{drop} = K$.) The full add/drop, with K = N, offers the most flexible routing, but may lead to excessive signal impairments or high cost of the complete OADM, so partial add/drops with $0.25 \le K/N \le 0.5$ have been proposed in a wide range of designs.[6]

However, specification of K and N is not a **complete** description of RWADM routing capability. Figure 1 shows a variety of RWADM designs with K = 4, N = 16 but very different routing abilities. The designs shown in Fig. 1 are not intended to be the best physical realizations; rather, they are schematic designs chosen to display some representative routing properties. Each design is based on a wavelength demultiplexer(DMUX) and multiplexer(MUX) pair with switches sandwiched in between, except for Fig. 1e, which uses a band-type DMUX/MUX pair with tunable single-wavelength couplers in between. The WADM of Fig. 1a offers the greatest flexibility, including access to any input wavelength, at the cost of a relatively large switch fabric. The WADMs of Fig. 1b, 1d use much smaller switch fabrics, and that of Fig. 1c uses an assembly of simple 2×2 switches. The WADMs of Fig. 1b, 2c allow add/drop of any or all wavelengths within a specific band of four, but the remaining 12 wavelengths are fixed in the express path. The design of Fig. 1d allows add/drop of any or all of four wavelengths in an equally-spaced comb pattern, while the design of Fig. 1e allows the add/drop of any single wavelength (or no wavelength) selected from each of four contiguous bands. Thus, the WADM of Fig. 1e can be set to add/drop any individual wavelength in the input spectrum (unlike the WADMs of Fig. 1b, 1c, 1d), but cannot add/drop any arbitrary combination of four wavelengths (unlike the WADM of Fig. 1a).

The limitations of the band-type designs (Fig. 1b, 1c, 1d) can be seen by considering a simple network example, shown in Fig. 3. The four-node ring with an all-to-all (logical mesh) traffic pat-